



UNIVERSITY OF LEEDS

This is a repository copy of *Screening and classifying small-molecule inhibitors of amyloid formation using ion mobility spectrometry-mass spectrometry*.

White Rose Research Online URL for this paper:  
<http://eprints.whiterose.ac.uk/85627/>

Version: Accepted Version

---

**Article:**

Young, LM, Saunders, JC, Mahood, RA et al. (6 more authors) (2015) Screening and classifying small-molecule inhibitors of amyloid formation using ion mobility spectrometry-mass spectrometry. *Nature Chemistry*, 7 (1). pp. 73-81. ISSN 1755-4330

<https://doi.org/10.1038/NCHEM.2129>

---

**Reuse**

Items deposited in White Rose Research Online are protected by copyright, with all rights reserved unless indicated otherwise. They may be downloaded and/or printed for private study, or other acts as permitted by national copyright laws. The publisher or other rights holders may allow further reproduction and re-use of the full text version. This is indicated by the licence information on the White Rose Research Online record for the item.

**Takedown**

If you consider content in White Rose Research Online to be in breach of UK law, please notify us by emailing [eprints@whiterose.ac.uk](mailto:eprints@whiterose.ac.uk) including the URL of the record and the reason for the withdrawal request.



[eprints@whiterose.ac.uk](mailto:eprints@whiterose.ac.uk)  
<https://eprints.whiterose.ac.uk/>

**Screening and classifying small molecule inhibitors of amyloid formation using ion mobility spectrometry-mass spectrometry**

**Lydia M. Young<sup>1,2#</sup>, Janet C. Saunders<sup>1,2#</sup>, Rachel A. Mahood<sup>1,2</sup>, Charlotte H. Revill<sup>1,3</sup>, Richard J. Foster<sup>1,3</sup>, Ling-Hsien Tu<sup>4</sup>, Daniel P. Raleigh<sup>4</sup>, Sheena E. Radford<sup>1,2\*</sup>, Alison E. Ashcroft<sup>1,2\*</sup>**

1. Astbury Centre for Structural Molecular Biology, University of Leeds, LS2 9JT, UK;
2. School of Molecular and Cellular Biology, University of Leeds, LS2 9JT, UK;
3. School of Chemistry, University of Leeds, LS2 9JT, UK;
4. Department of Chemistry, Stony Brook University, Stony Brook, NY 11794-3400, USA.

# These authors contributed equally to this work.

\*Corresponding authors:

email: [s.e.radford@leeds.ac.uk](mailto:s.e.radford@leeds.ac.uk) and [a.e.ashcroft@leeds.ac.uk](mailto:a.e.ashcroft@leeds.ac.uk)

## ***Supplementary Information***

## **Contents**

Section 1: Selection of small molecules used for screen validation .....	3
Table S1: Molecular masses of small molecules initially screened .....	4
Section 2: Expression and purification of recombinant hIAPP and A $\beta$ 40 .....	5
Figure S1: hIAPP monomer drift times in the absence or presence of FG .....	7
Figure S2: Ionic strength-dependence of ligand binding to hIAPP .....	8
Figure S3: ESI-MS spectrum of hIAPP with tramiprosate .....	9
Figure S4: ESI-MS spectrum of Congo red alone .....	10
Figure S5: Molecules that do not inhibit hIAPP aggregation .....	11
Figure S6: LogP values of the ten compounds selected for initial analysis .....	12
Figure S7: Collision induced dissociation (CID) of ligand bound to hIAPP .....	13
Figure S8: ESI-IMS-MS ATDs of hIAPP in the absence and presence of inhibitors .....	14
Figure S9: ESI-MS and ESI-IMS-MS of hIAPP with mixtures of small molecules (1) .....	15
Figure S10: ESI-MS and ESI-IMS-MS of hIAPP with mixtures of small molecules (2) .....	16
Table S2: Focused high throughput screen (HTS) results .....	17
Figure S11. LogP values of the 20 compounds identified from the focused screen plus ten other small molecules .....	20
Figure S12. ROCS-derived overlay of molecule number 26 with chloronaphthoquinine–tryptophan .....	21
Figure S13. ESI-IMS-MS analysis of ‘hit’ compound number 26 .....	22
Figure S14. Proof of principle 96-well plate automated semi-HTS .....	23
References .....	24

## **Section 1: Selection of small molecules used for screen validation**

**'Positives'**: Fast green FCF (FG) (**1**), a triarylmethane food dye, has been shown previously to inhibit amyloid formation by hIAPP<sup>1</sup> and is used here as an example of inhibition by specific binding. Previous studies have shown that EGCG<sup>2-6</sup> (**2**) and silibinin<sup>2,7</sup> (**3**) also act as specific inhibitors of hIAPP amyloid formation and are included here for comparison. EGCG is the most well characterised 'positive' aggregation inhibitor of a variety of proteins (e.g.  $\alpha$ -synuclein<sup>8</sup>, hIAPP<sup>2-6</sup> and A $\beta$ 40/42<sup>3,8-10</sup>) both *in vitro* and *in vivo*<sup>3,8,9,11-14</sup>. In contrast, to our knowledge, silibinin has only been reported to inhibit hIAPP self-assembly<sup>2,7</sup>.

**'Colloidal'**: Congo red (CR) (**4**), a dye commonly used to detect the presence of amyloid fibrils, was initially reported to bind to numerous protein aggregates<sup>15-17</sup>, prevent aggregation *in vitro*<sup>18,19</sup> and reduce neurotoxicity *in vivo*<sup>20,21</sup>. It has since been reported, however, to function via a colloidal mechanism<sup>22</sup>. This mode of inhibition is likely due to the ability of CR to self-assemble into micelle-like species, driven by stacking of its aromatic rings<sup>23</sup>.

**'Non-specific'**: 1*H*-benzimidazole-2-sulfonic acid (1*H*-B-SA) (**5**), previously not assessed against hIAPP, was included in the analysis as it possesses a sulfonic acid moiety and is aromatic in nature. Tramiprosate (**6**) has been used as a negative control for hIAPP inhibition *in vitro*<sup>1,24</sup>.

**'Negatives'**: The non-steroidal anti-inflammatory (NSAID) compounds aspirin (**7**) and ibuprofen (**8**), plus benzimidazole (**9**) and hemin (**10**), contain charged and/or aromatic functional groups which are prevalent in known amyloid inhibitors, but have not previously been assessed for their interaction with hIAPP. Aspirin has been reported to inhibit fibrillogenesis of A $\beta$ 40 and A $\beta$ 42<sup>25,26</sup>, and ibuprofen to reduce cognitive deficits *in vivo*<sup>27,28</sup> and also to reduce A $\beta$  aggregation *in vitro*<sup>29,30</sup>. Benzimidazole was used in the screen described here to determine whether the non-specific interaction observed between hIAPP and 1*H*-B-SA results from the presence of a negatively charged sulfonated group interacting with the positively charged hIAPP in the gas-phase. Hemin has been reported previously to inhibit fibrillogenesis of A $\beta$ <sup>19,31</sup>, however, it has not been assessed for its interactions with hIAPP or any effect on self-assembly.

No.	Compound	Average MW (Da)
1	<b>Fast Green FCF</b> ethyl-[4-[[4-[ethyl-(3-sulfophenyl) methyl] amino] phenyl)-(4-hydroxy-2-sulfophenyl) methylidene]-1-cyclohexa-2,5-dienylidene]-[(3-sulfophenyl) methyl] azanium	765.9
2	<b>EGCG</b> [(2 <i>R</i> ,3 <i>R</i> )-5,7-dihydroxy-2-(3,4,5-trihydroxy-phenyl) chroman-3-yl] 3,4,5-trihydroxybenzoate	458.4
3	<b>Silibinin</b> (2 <i>R</i> ,3 <i>R</i> )-3,5,7-trihydroxy-2-[(2 <i>R</i> ,3 <i>R</i> )-3-(4-hydroxy-3-methoxyphenyl)-2-(hydroxymethyl)-2,3-dihydrobenzo[ <i>b</i> ][1,4]dioxin-6-yl]chroman-4-one	482.4
4	<b>Congo red</b> 4-amino-3-[4-[4-(1-amino-4-sulfonato-naphthalen-2-yl) diazenylphenyl]phenyl] diazenyl-naphthalene-1-sulfonate	652.7
5	<b>1<i>H</i>-B-SA</b> 1 <i>H</i> -benzimidazole-2-sulfonic acid	198.2
6	<b>Tramiprosate</b> 3-Aminopropane-1-sulfonic acid	139.2
7	<b>Aspirin</b> 2-acetoxybenzoic acid	180.2
8	<b>Ibuprofen</b> ( <i>RS</i> )-2-(4-(2-methylpropyl)phenyl)propanoic acid	206.3
9	<b>Benzimidazole</b> 1 <i>H</i> -benzimidazole	118.1
10	<b>Hemin</b> chloro[3,7,12,17-tetramethyl-8,13-divinylporphyrin-2,18-dipropanoato(2-)]iron(III)	651.9

**Table S1. Molecular masses of small molecules initially screened, confirmed as  $MH^+$  ions using ESI-IMS.**

## **Section 2: Expression and purification of recombinant hIAPP and A $\beta$ 40**

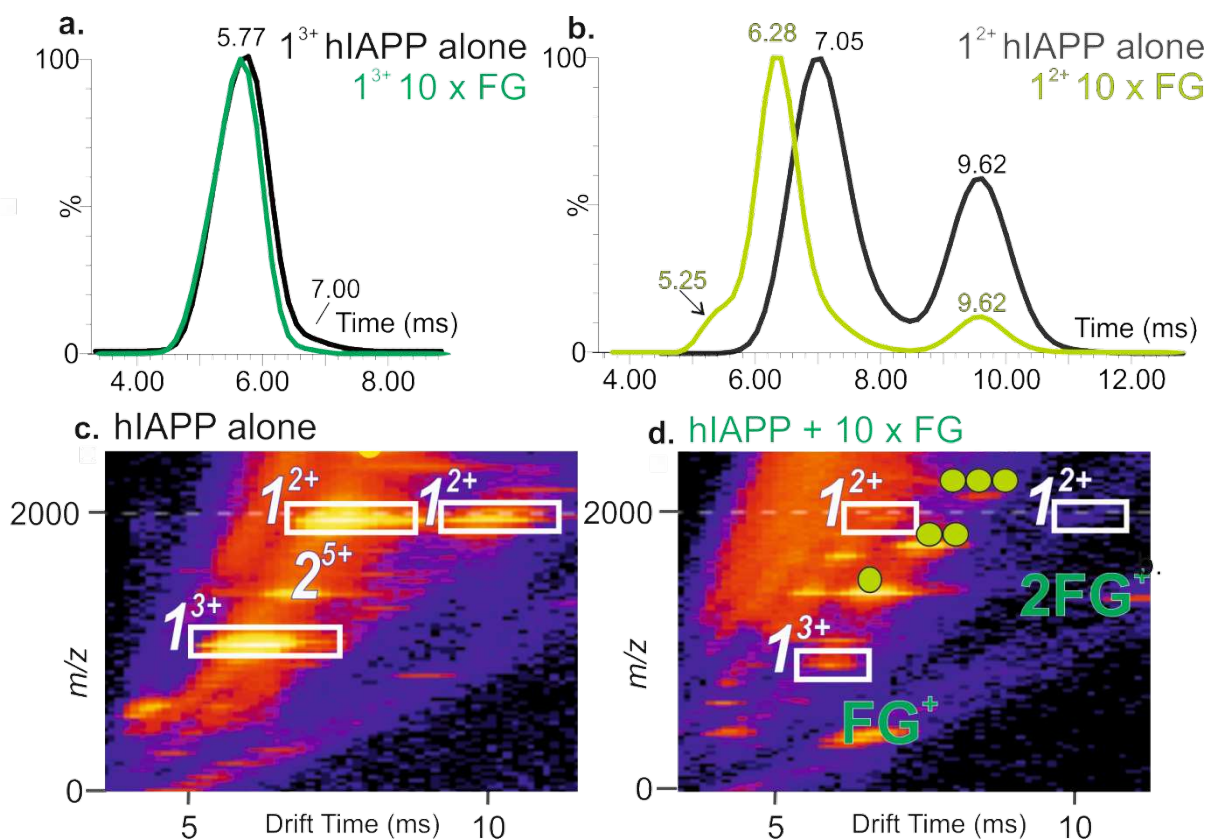
### ***hIAPP synthesis and purification***

Human IAPP was synthesized on a 0.1 mmol or 0.25 mmol scale using a CEM Liberty peptide synthesizer, and 9-fluorenylmethoxycarbonyl (Fmoc) chemistry. Fmoc protected pseudoproline dipeptide derivatives were incorporated to facilitate the synthesis<sup>32</sup>. 5-(4'-fmoc-aminomethyl-3', 5-dimethoxyphenol) valeric acid (PAL-PEG) resin was used to generate an amidated C-terminus. Double couplings were performed for the first residue attached to the resin, pseudoprolines, all  $\beta$ -branched residues and all residues directly following a  $\beta$ -branched residue. Peptides were cleaved from the resin through the use of standard trifluoroacetic acid (TFA) methods. Crude peptides were dissolved in 20% acetic acid (v/v), frozen in liquid nitrogen and lyophilized to increase their solubility. The disulfide bond was formed via oxidation by use of DMSO<sup>33</sup>. Peptides were purified by reverse-phase HPLC using a Vydac C18 preparative column (10 mm x 250 mm) with buffer A, consisting of 100% H<sub>2</sub>O and 0.045% HCl (v/v) and buffer B, composed of 80% acetonitrile, 20% H<sub>2</sub>O and 0.045% HCl. HCl was used as the ion-pairing agent since residual TFA can cause problems with cell toxicity assays and can influence the aggregation kinetics of some amyloidogenic peptides<sup>34</sup>. The identity of the pure products was confirmed by mass spectrometry using a Bruker MALDI-TOF MS: human IAPP: expected 3903.3 Da, observed 3903.5 Da. Analytical HPLC was used to confirm the purity of the peptides before each experiment. This is an important control because deamidation alters the aggregation of hIAPP<sup>35,36</sup>.

### ***A $\beta$ (M1-40) synthesis and purification***

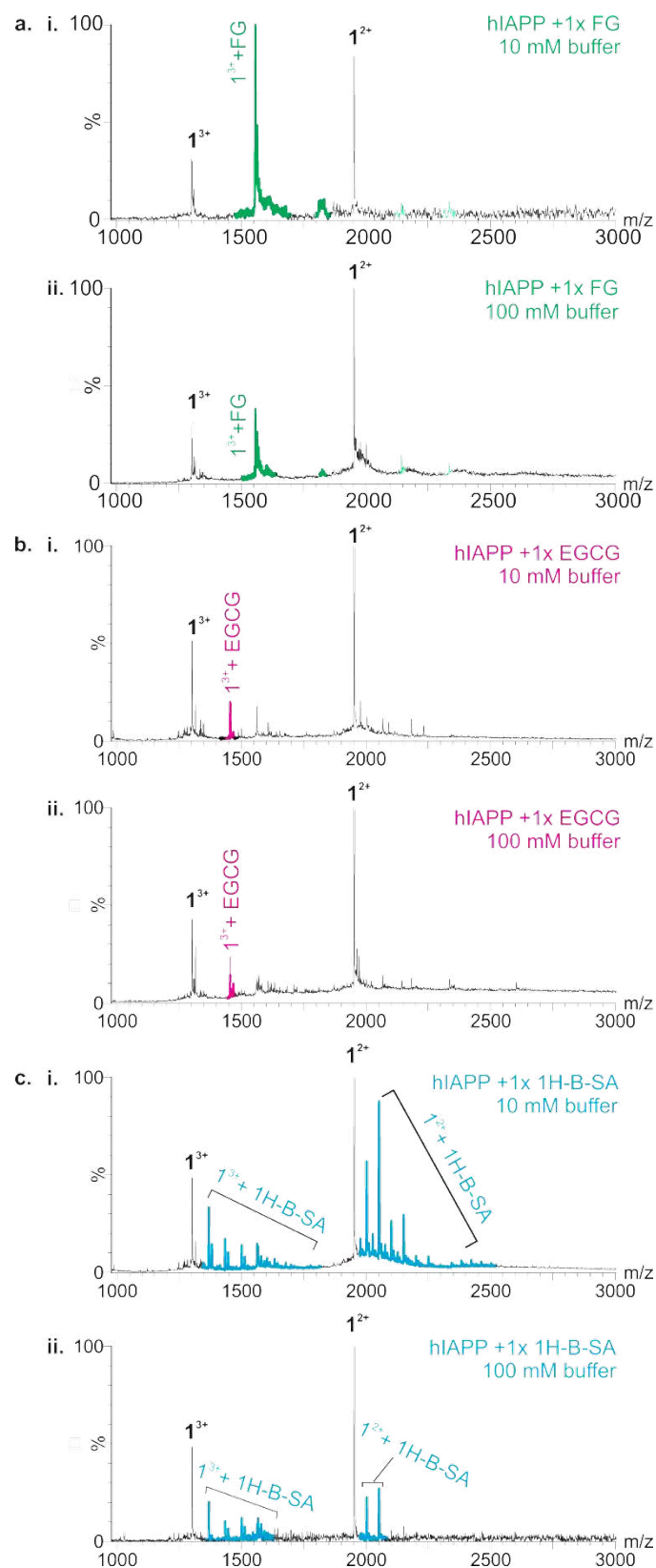
A $\beta$ (M1-40) was expressed in BL21 [DE3] pLysS cells (Agilent) from a PetSac vector, kindly provided by Dominic Walsh (Brigham & Women's Hospital, Boston, USA) and Sara Linse (Lund University, Sweden). Cells were grown at 37 °C in LB media, containing ampicillin (100  $\mu$ g/mL) and chloramphenicol (25  $\mu$ g/mL). Expression of A $\beta$ (M1-40) was induced by the addition of 0.5 mM isopropyl- $\beta$ -D-thiogalacto-pyranoside at an OD<sub>600</sub> of 0.5, followed by a 3 h incubation at 37 °C. Cells were collected by centrifugation (Beckman-Coulter JLA 8.1, 6000 g, 15 min, 4 °C) and purified using a modified protocol provided by Walsh *et al.*<sup>37</sup>. Briefly, cells were disrupted in 10 mM Tris-HCl, 1 mM EDTA, pH 8.5, containing 20  $\mu$ g/mL DNase, 1 mM phenylmethanesulfonyl fluoride and 2 mM benzamidine. The suspension was stirred at 4 °C for 1 h before homogenization and sonication (30 s, 4 W). The extract was then centrifuged (Beckman-Coulter JA 25.5, 20,000 g, 15 min, 4 °C). The pellet was resuspended in 10 mM Tris-HCl, pH 8.5, containing 8 M urea and sonicated to dissolve the inclusion bodies. The suspension was centrifuged again and the supernatant collected, diluted 1:4 in 10 mM Tris-HCl buffer and agitated gently with Q Sepharose Fast Flow resin (GE Healthcare, Amersham, Bucks, UK.) for 30 min. After washing the resin with buffer containing 0 mM NaCl and then 25 mM NaCl, peptide-enriched fractions were eluted with 125 mM NaCl, dialysed into 50 mM ammonium bicarbonate, pH 8.0 and lyophilized. Semi-purified A $\beta$ (M1-40) was resolubilized in 50 mM Tris-HCl containing 7 M GuHCl, pH 8.5 at a concentration of approximately 10 mg/mL and purified by size exclusion chromatography (HiLoad Superdex 75 26/60 column, GE Healthcare, Amersham, Bucks, UK) into 50 mM ammonium hydrogen carbonate before finally lyophilizing and storing at -20 °C.

**Figure S1: hIAPP monomer drift times in the absence or presence of FG**



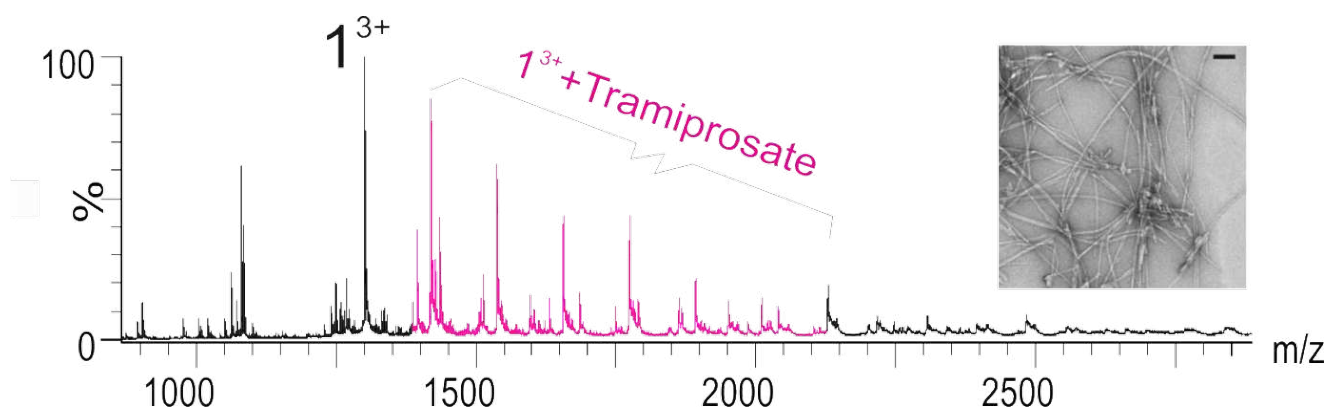
**Figure S1.** Comparisons of hIAPP monomer drift times in the absence (black) or presence (green) of excess FG. (a) Arrival time distribution (ATD) of the hIAPP 3+ monomer ions displays one distinct conformer (drift time = ~5.8 ms) and a small component of a more extended conformation (drift time = ~7.0 ms) in the absence and presence of FG; (b) Arrival time distribution (ATD) of the hIAPP 2+ monomer ions displays two distinct conformers in the absence of FG (drift times = ~7.1 and ~9.6 ms). In the presence of FG, the hIAPP 2+ monomer displays three distinct conformers (drift times = ~5.3, ~6.3 and ~9.6 ms); (c) ESI-IMS-MS Driftscope plots of monomeric conformers observed for hIAPP alone; and (d) when FG is present at a 10-fold molar excess over hIAPP. Monomer peaks are enclosed by white boxes. Circles represent number of FG molecules bound to each species.

**Figure S2: Ionic strength-dependence of ligand binding to hIAPP**



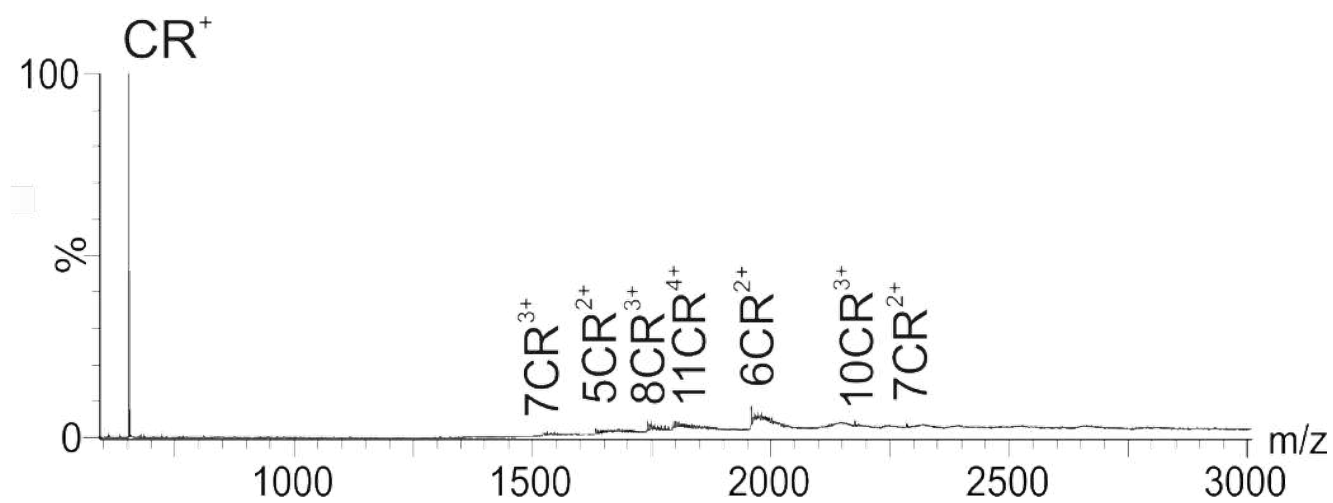
**Figure S2.** Positive ion ESI mass spectra showing (a) FG; (b) EGCG; and (c) 1H-B-SA added at a 1:1 molar ratio to hIAPP (32  $\mu$ M) in 10 mM (a. i, b. i, c. i) or 100 mM (a. ii, b. ii, c. ii) ammonium acetate buffer, pH 6.8. Ligand bound peptide peaks are highlighted in green (FG), pink (EGCG) and blue (1H-B-SA).

**Figure S3: ESI-MS spectrum of hIAPP with tramiprosate**



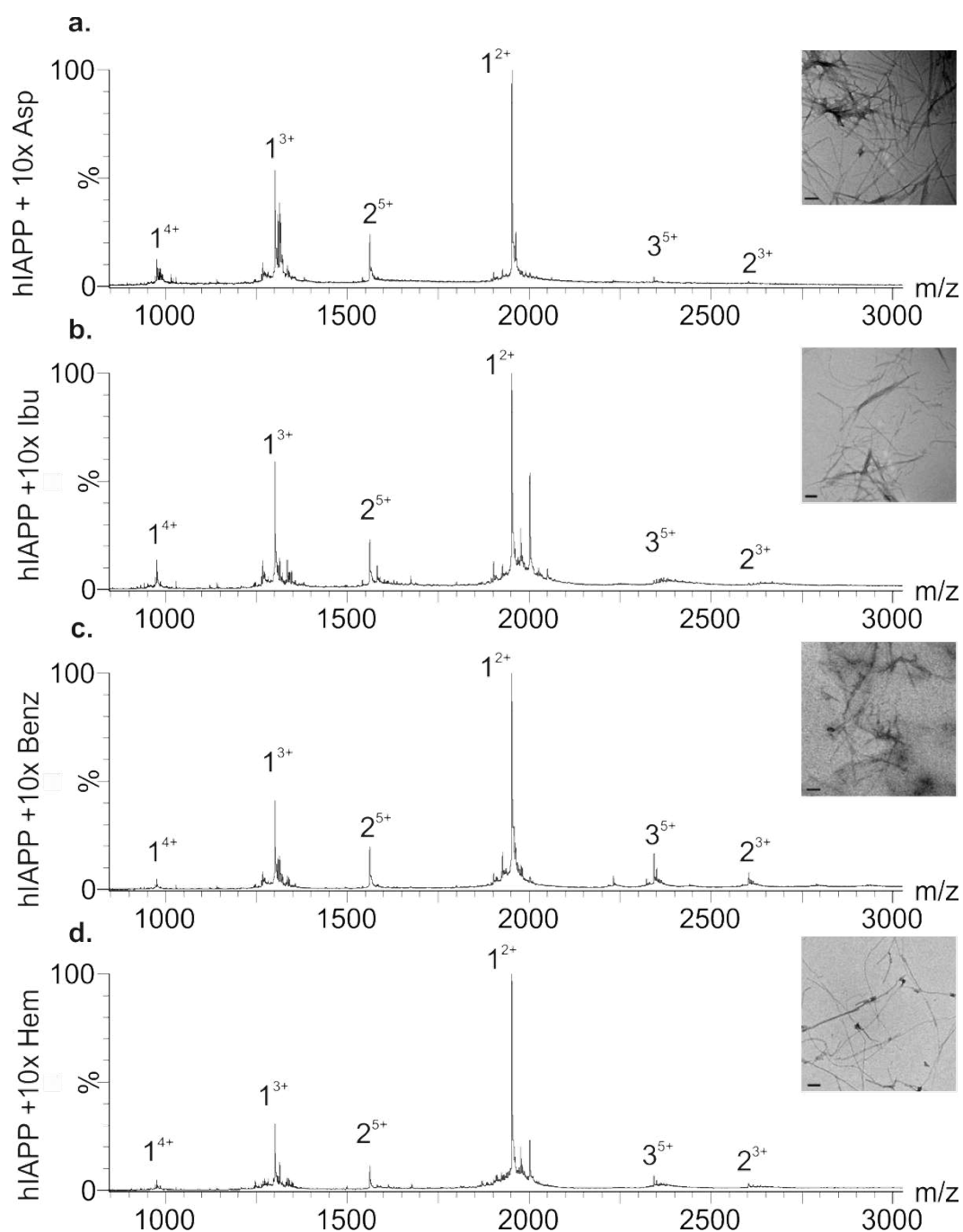
**Figure S3.** ESI-MS spectrum of hIAPP (32  $\mu\text{M}$ ) in the presence of tramiprosate (320  $\mu\text{M}$ ). Protein-ligand bound peaks are colored pink. Inset shows negative stain TEM image of fibrils formed by hIAPP when incubated with a 10:1 molar ratio of tramiprosate:hIAPP for 5 days (25  $^{\circ}\text{C}$ , quiescent) (scale bar = 500 nm).

**Figure S4: ESI-MS spectrum of Congo red alone**



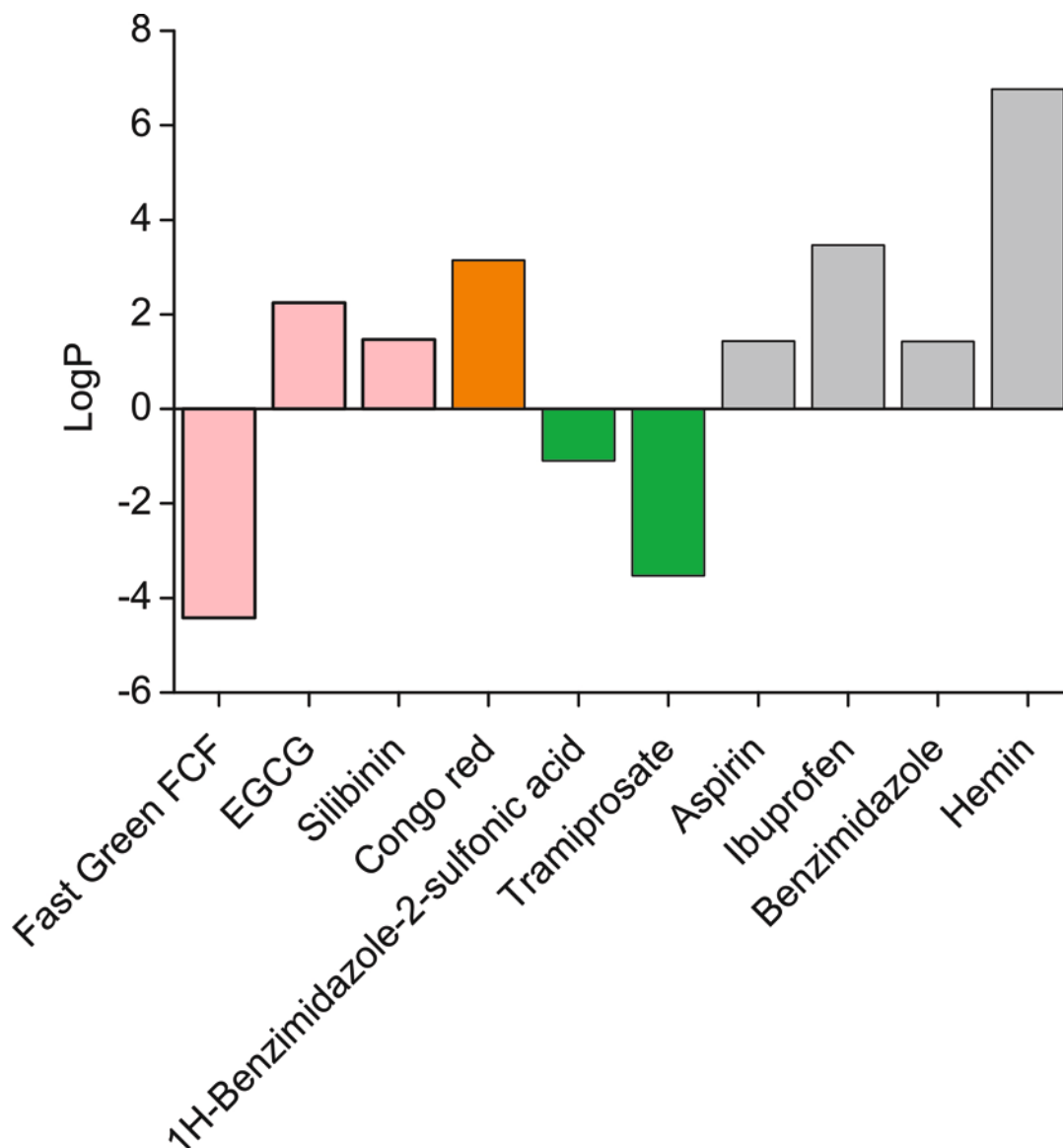
**Figure S4.** ESI-MS spectrum of 320  $\mu\text{M}$  Congo red (200 mM ammonium acetate, pH 6.8), showing self-aggregation (5- to 11-mers).

**Figure S5: Molecules that do not inhibit hIAPP aggregation**



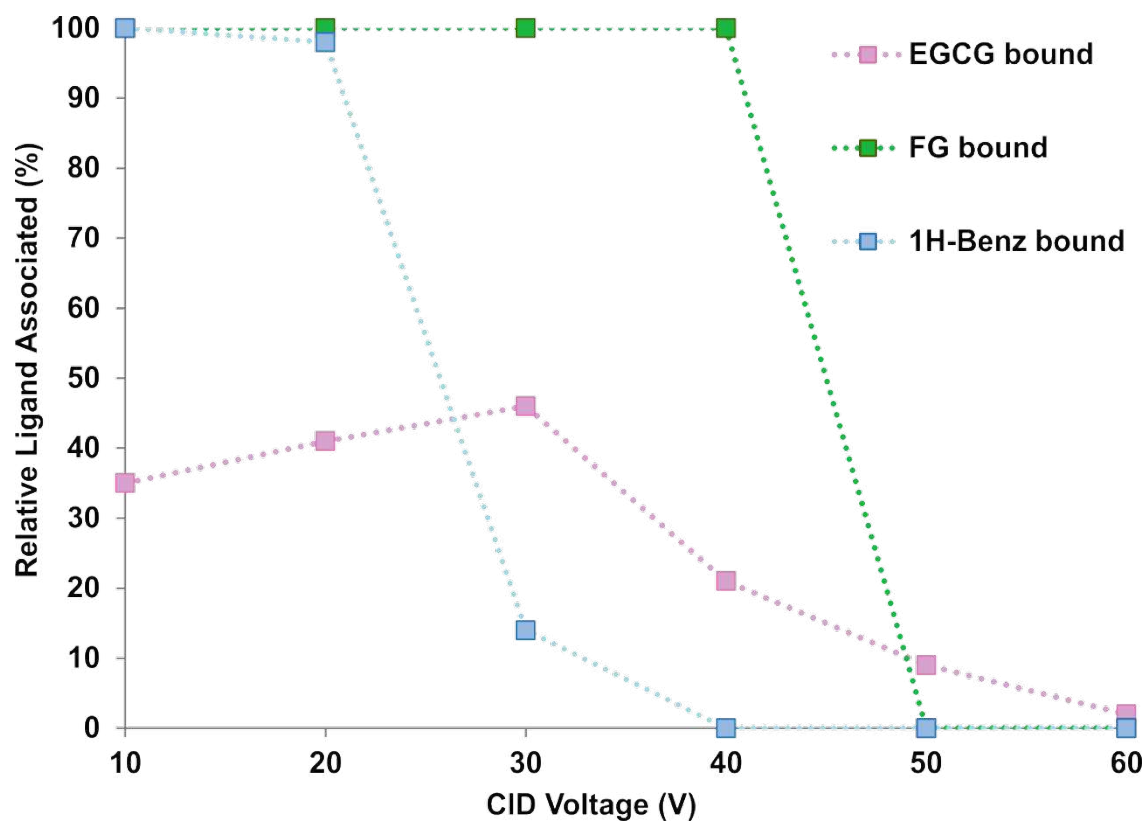
**Figure S5.** Lack of inhibition of hIAPP amyloid assembly by (a) aspirin; (b) ibuprofen; (c) benzimidazole; and (d) hemin. Positive ion ESI mass spectra showing no observed binding when each small molecule is added at 320  $\mu\text{M}$  to hIAPP peptide (32  $\mu\text{M}$ ). Insets: negative stain TEM images of hIAPP incubated with 10:1 molar ratios of small molecule:hIAPP for 5 days (25  $^{\circ}\text{C}$ , quiescent) (scale bar = 100 nm).

**Figure S6: LogP values of the ten compounds selected for initial analysis**



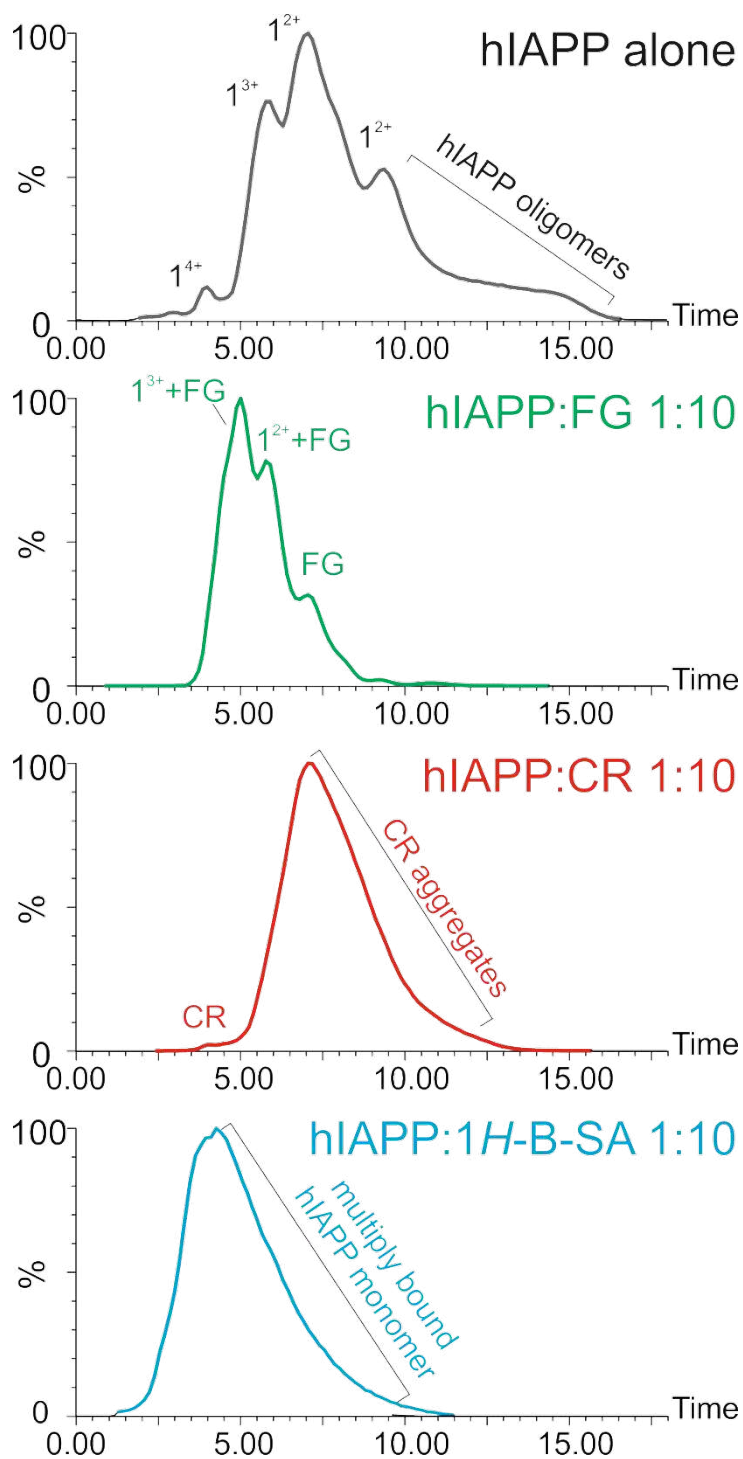
**Figure S6.** LogP values (the log of the hydrophobic/aqueous partition coefficient) were calculated for the ten small molecules (Table S1) using [www.molinspiration.com](http://www.molinspiration.com) software, which determines the hydrophobic parameters of the substituents. Molecules with high LogP values have high hydrophobicity. Colors denote inhibitor classification: positive (pink), colloidal (orange), non-specific (green) and negative (gray).

**Figure S7: Collision induced dissociation (CID) of ligand bound to hIAPP**



**Figure S7.** Differences between peptide-ligand complex stabilities in the gas-phase measured using Collision Induced Dissociation (CID). CID MS/MS of FG-hIAPP (green), EGCG-hIAPP (pink) and 1H-Benz-hIAPP (blue) complexes (32  $\mu$ M peptide, 320  $\mu$ M ligand, 200 mM ammonium acetate buffer, pH 6.8). Relative intensity of the 2+ monomer ions bound to ligand is plotted versus increasing ion-accelerating voltage into the trap collision cell.

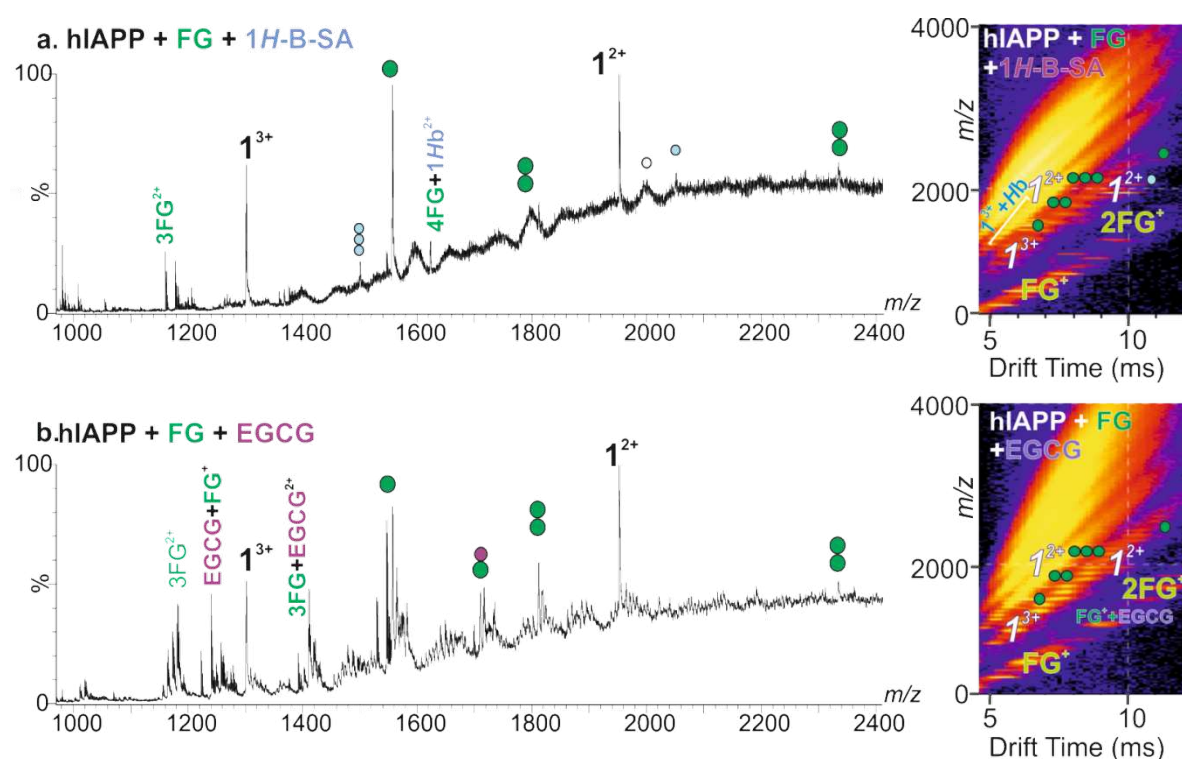
**Figure S8: ESI-IMS-MS ATDs of hIAPP in the absence and presence of inhibitors**



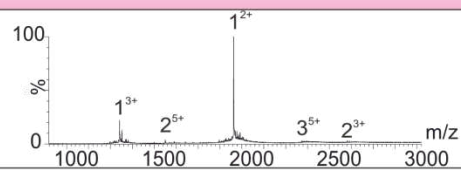
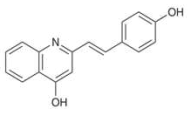
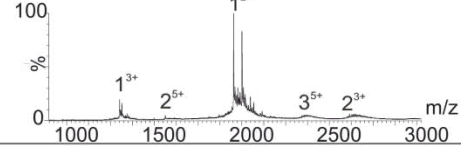
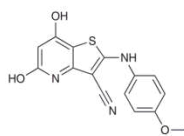
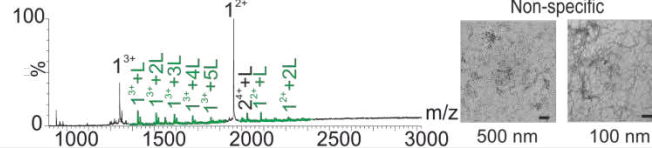
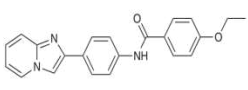
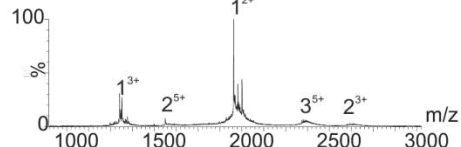
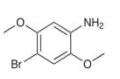
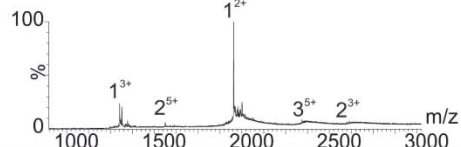
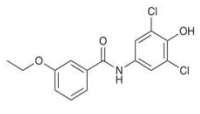
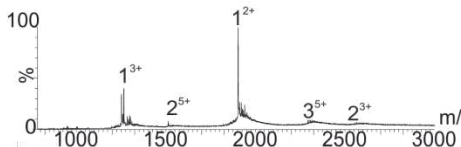
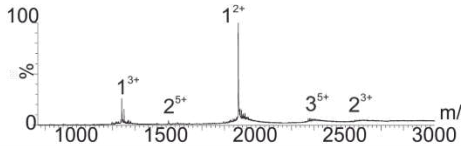
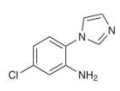
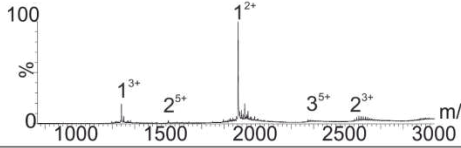
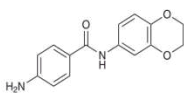
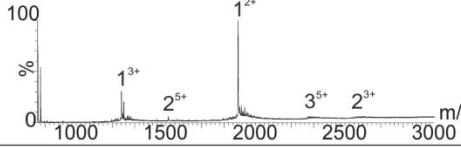
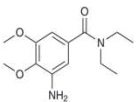
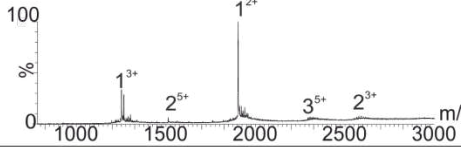
**Figure S8.** ATDs of hIAPP in the absence or presence of inhibitors. Comparisons of whole spectra arrival time distributions (ATDs) of hIAPP in the absence (grey) or presence of a 10-fold molar excess of FG (green), CR (red) or 1H-B-SA (blue).



**Figure S10: ESI-MS and ESI-IMS-MS of hIAPP with mixtures of small molecules (2)**



**Figure S10.** Positive ion ESI mass spectra and IMS-MS Driftscope plots showing hIAPP peptide (32  $\mu\text{M}$ ) in solution with mixtures of compounds. (a) hIAPP with Fast Green FCF (FG) (160  $\mu\text{M}$ ) and 1H-benzimidazole-2-sulfonic acid (1H-B-SA) (160  $\mu\text{M}$ ), FG bound monomer peaks denoted with green circles and a white circle when dimer bound, 1H-B-SA bound monomer peaks denoted with blue circles; (b) hIAPP with Fast Green FCF (160  $\mu\text{M}$ ) and EGCG (160  $\mu\text{M}$ ). FG bound monomer peaks are denoted with green circles. EGCG bound peaks are denoted with purple circles. Number of circles represents number of ligands bound.

Mol N°	Small Molecule	Structure	Mass Spectra	Classification
11	(2-isopropoxyphenyl) amine			Negative
12	2-[2-(4-hydroxyphenyl) vinyl]-4-quinolinol			Negative
13	5,7-dihydroxy-2-[(4-methoxyphenyl)amino]thieno[3,2-b]pyridine-3-carbonitrile			Non-specific
14	4-ethoxy-N-(4-imidazo [1,2-a] pyridin-2-yl)phenyl benzamide			Negative
15	(4-bromo-2,5-dimethoxyphenyl) amine			Negative
16	N-(3,5-dichloro-4-hydroxyphenyl)-3-ethoxybenzamide			Negative
17	[1,2,4]triazolo[1,5-a][1,3,5]triazin-7-amine			Negative
18	5-Chloro-2-(1H-imidazol-1-yl)aniline			Negative
19	4-amino-N-(2,3-dihydro-1,4-benzodioxin-6-yl)benzamide			Negative
20	3-amino-N,N-diethyl-4,5-dimethoxybenzamide			Negative

**Table S2: Focused high throughput screen (HTS) results.** Molecule number **26** inhibits hIAPP aggregation by specific binding (red peaks); compounds **13**, **25**, **27** exhibit non-specific binding (green peaks). TEMs are shown only for compounds in which binding is observed (scale bar in nm is indicated at the foot of each TEM image).

Mol N°	Small Molecule	Structure	Mass Spectra	Classification
21	N-(3-hydroxyphenyl)-3,4-dimethoxybenzamide			Negative
22	3-amino-N-cyclopropyl-4-methoxybenzamide			Negative
23	1-[4-(hydroxy-2-methyl-3-[(4-phenyl-1-piperazinyl)methyl]-6-quinolinyl)ethanone			Negative
24	3,5-dimethoxy-N-[4-(8-methylimidazo[1,2-a]pyridin-2-yl)phenyl]benzamide			Negative
25	N-(2,3-dihydro-1,4-benzodioxin-6-yl)-2-[(4-methyl-6-oxo-1,6-dihydropyrimidin-2-yl)amino]piperidin-1-yl]acetamide			Non-specific 
26	6-[[4-(2-fluorophenyl)-1-piperazinyl]carbonyl]-3-methyl-5H-[1,3]thiazolo[3,2-a]pyrimidin-5-one			Positive 
27	1-(Adamantan-1-ylcarbonyl)-1'H-spiro[piperidine-4,2'-quinazolin]-4'(3'H)-one			Non-specific 
28	N-(5-Methoxy-2-methyl-1,3-benzothiazol-4-yl)acetamide			Negative
29	1-(2,3-dimethoxybenzoyl)-4-ethylpiperazine(phenyl)-benzamide			Negative
30	N-(4-aminophenyl)-2-bromobenzamide			Negative

**Table S2 continued.**

Mol N°	Small Molecule	Structure	Mass Spectra	Classification
31	<b>L-DOPA</b> (L-3,4-dihydroxyphenylalanine)			Negative
32	<b>Neocuprione</b> (2,9-dimethyl-1,10-phenanthroline)			Negative
23	<b>Lacmoid</b> (7-amino-2,8-bis(2,4-dihydroxyphenyl)-phenoxazin-3-one)			Negative
34	<b>Hematin</b> (hydroxy[3,7,12,17-tetramethyl-8,13-divinylporphyrin-2,18-dipropanoato(2-)(iron III)])			Negative
35	<b>Melatonin</b> (N-(2-(5-methoxy-14-ind-3-yl)ethyl)acetamide)			Negative
36	<b>Chloragenic acid</b> (((1S,3R,4R,5R)-3-(((Z)-3-(3,4-dihydroxyphenyl)prop-2-enyl)oxy)-1,4,5-trihydroxycyclohexane-carboxylic acid))			Negative
37	<b>2-Amino-methylbenzimidazole</b>			Negative
38	<b>2,3,4-Trihydroxybenzophenone</b>			Negative
39	<b>Ibuprofen</b> (((R,S)-2-(4-(2-methylpropyl)phenyl)propanoic acid))			Negative
40	<b>Azure C</b> (3-Amino-7-(methylamino)phenothiazin-5-ium chloride)			Negative

**Table S2 continued.**

**Figure S11: LogP values of the 20 compounds identified from the focused screen and 10 other small molecules**

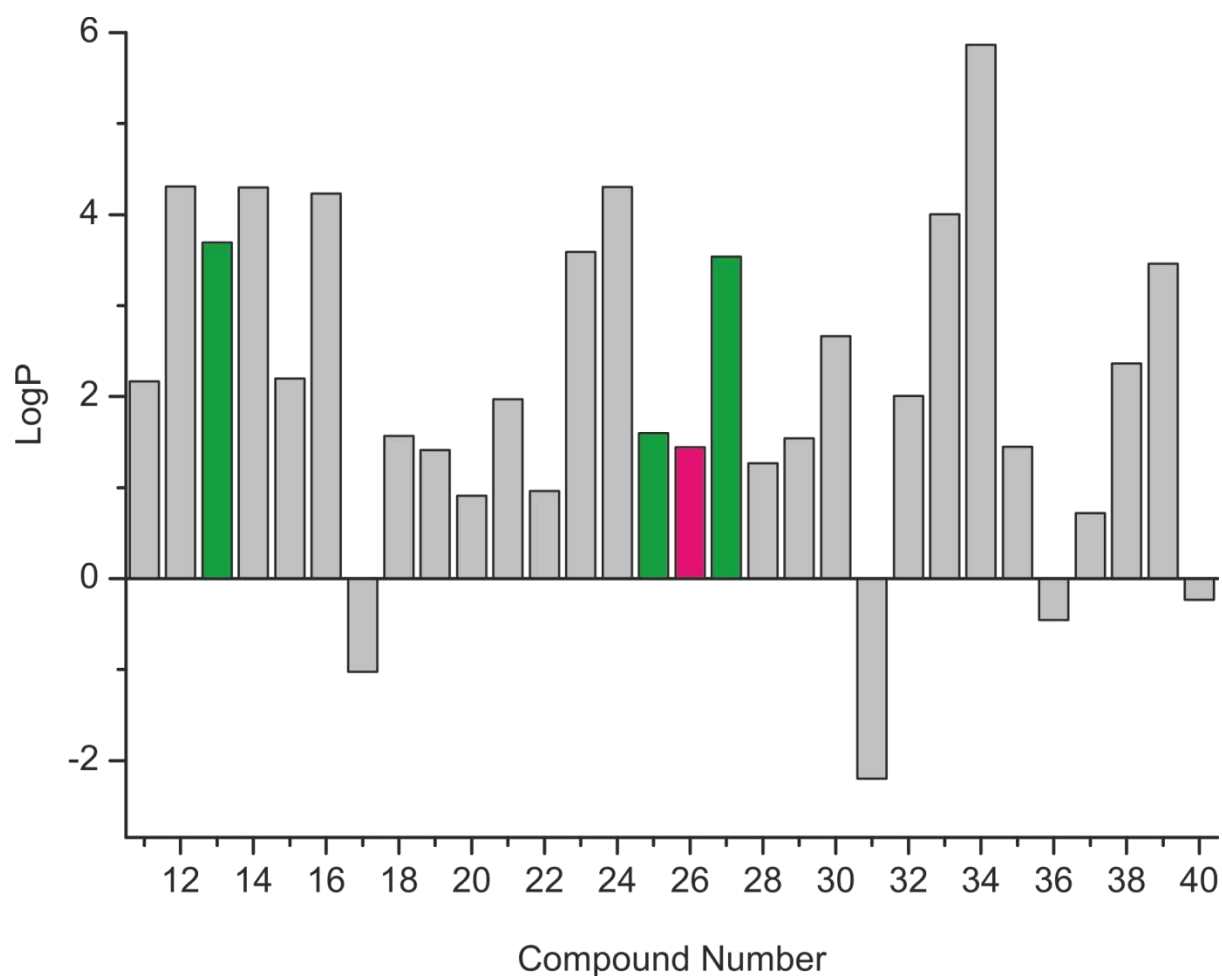


**Figure S11.** LogP values (the log of the hydrophobic/aqueous partition coefficient) were calculated for the 20 small molecules identified from the focused screen (compounds **11-30**) using [www.molinspiration.com](http://www.molinspiration.com) software, which determines the hydrophobic parameters of the substituents, plus 10 other small molecules reported to inhibit amyloid formation by other polypeptide sequences (compounds **31-40**). Molecules with high LogP values have high hydrophobicity. Colors denote inhibitor classification: positive (pink), non-specific (green) and negative (gray).

**Figure S12: ROCS-derived overlay of molecule number 26 with chloronaphthoquinine–tryptophan**

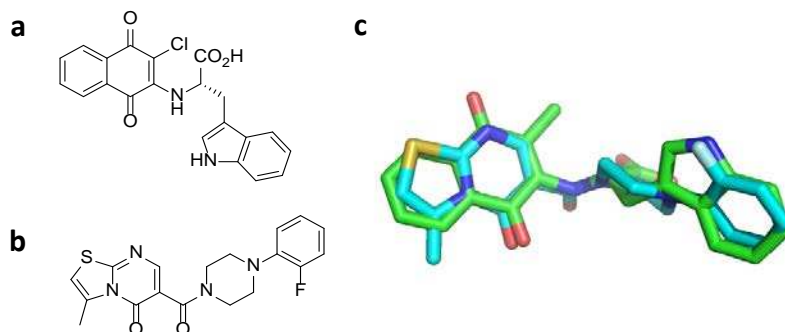


**Figure S12.** (a) Chemical structure of chloronaphthoquinine–tryptophan; (b) chemical structure of molecule number **26**; (c) ROCS-derived overlay of chloronaphthoquinine–tryptophan (green sticks) and molecule number **26** (cyan sticks).

**Figure S13: ESI-IMS-MS analysis of 'hit' compound number 26**

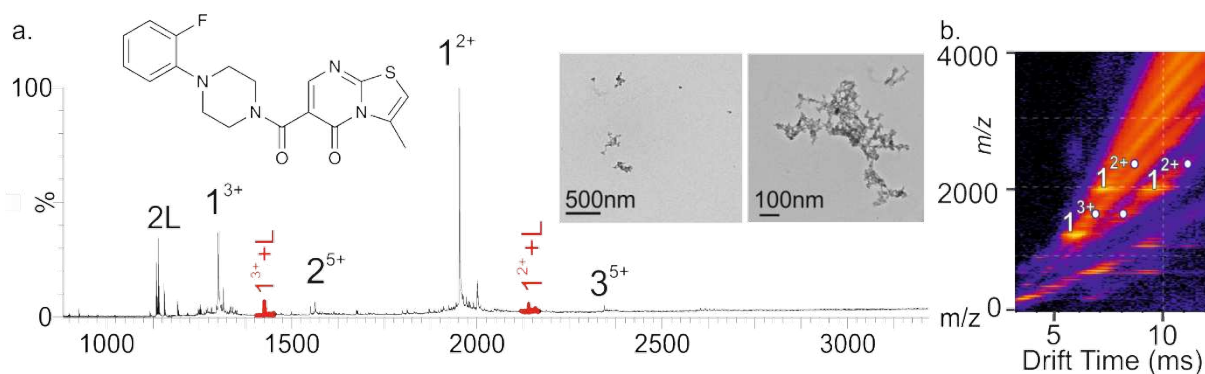


**Figure S13.** Inhibition of hIAPP fibril formation by compound **26**. (a) Positive ion ESI mass spectrum showing binding of compound **26** (6-[[4-(2-fluorophenyl)-1-piperazinyl]carbonyl]-3-methyl-5H-[1,3]thiazolo[3,2-a]pyrimidin-5-one) (added at 320  $\mu\text{M}$  to 32  $\mu\text{M}$  peptide) to both the +2 and +3 charge state ions of hIAPP monomer (bound peaks coloured red). The structure of compound **26** and negative stain TEM images of hIAPP incubated with 10:1 molar ratios of molecule:hIAPP for 5 days (25  $^{\circ}\text{C}$ , quiescent) are inset; (b) ESI-IMS-MS Driftscope plot shows hIAPP species detected in the presence a 10:1 molar ratio of compound **26**:peptide monomer at  $t = 2$  min. Bound monomer peaks are denoted with a white circle.

### Figure S14. Proof of principle 96-well plate automated semi-HTS

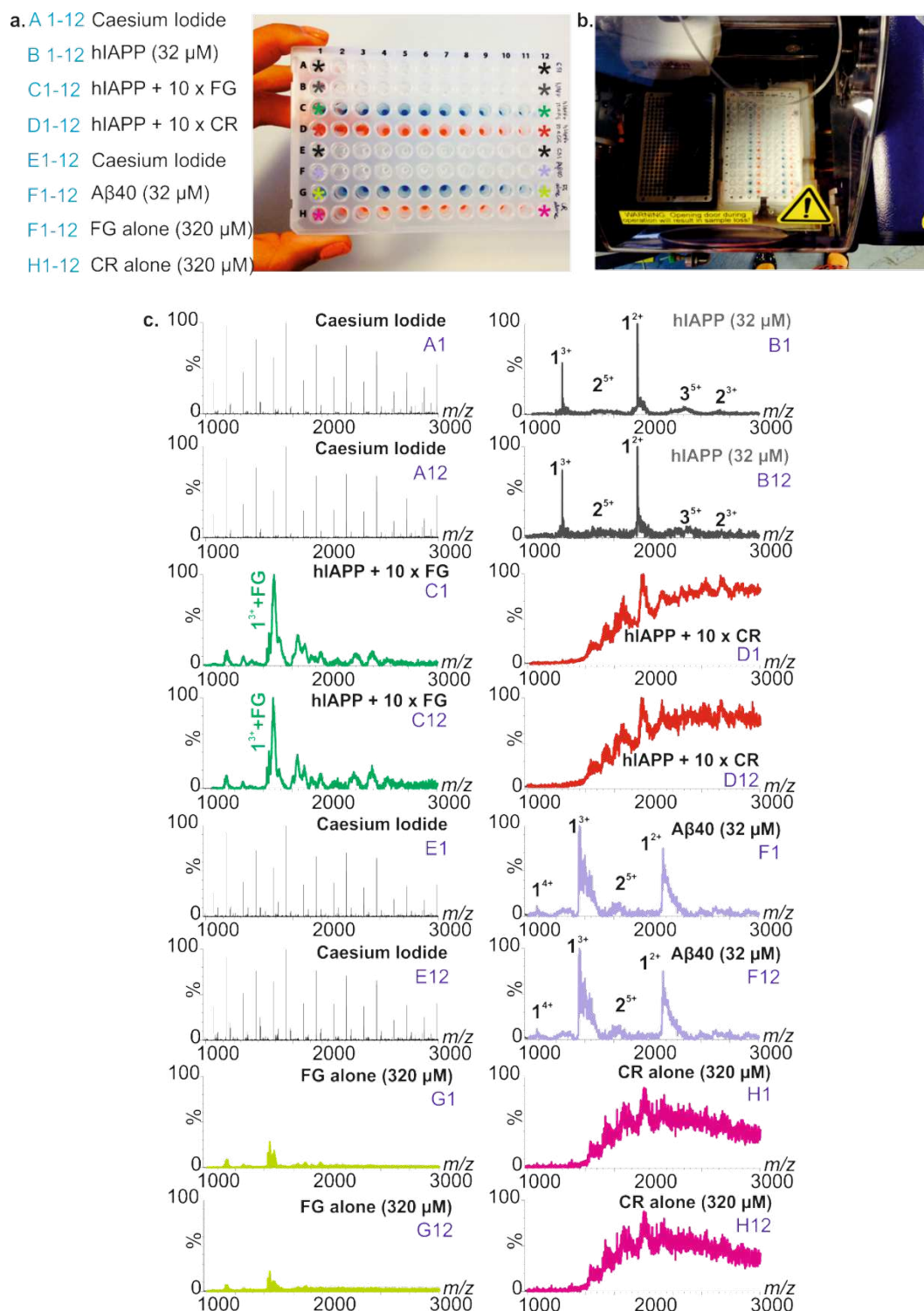


**Figure S14.** Proof of principle 96-well plate automated semi-HTS by ESI-MS. (a) 10  $\mu$ L samples containing aqueous CsI (A/E 1-12) for calibration, hiAPP (B1-12), hiAPP:FG (C1-12) hiAPP:CR (D1-12), A $\beta$ 40 (F1-12), FG alone (G1-12), and CR alone (H1-12) were prepared in 96-well plates. Peptide samples (32  $\mu$ M) were dissolved in 200 mM ammonium acetate (pH 6.8) in the absence or presence of 320  $\mu$ M small molecule; (b) samples were infused into the mass spectrometer via a Triversa NanoMate automated nano-ESI interface; (c) spectra resulting from the first and twelfth well of each row of the 96-well plate (annotated A1, A12, respectively) demonstrate the reproducibility of the assay.

## References

- 1 Meng, F. *et al.* The sulfated triphenyl methane derivative acid fuchsin is a potent inhibitor of amyloid formation by human islet amyloid polypeptide and protects against the toxic effects of amyloid formation. *J. Mol. Biol.* **400**, 555-566, (2010).
- 2 Young, L. M., Cao, P., Raleigh, D. P., Ashcroft, A. E. & Radford, S. E. Ion mobility spectrometry-mass spectrometry defines the oligomeric intermediates in amylin amyloid formation and the mode of action of inhibitors. *J. Am. Chem. Soc.* **136**, 660-670, (2014).
- 3 Palhano, F. L., Lee, J., Grimster, N. P. & Kelly, J. W. Toward the molecular mechanism(s) by which EGCG treatment remodels mature amyloid fibrils. *J. Am. Chem. Soc.* **135**, 7503-7510, (2013).
- 4 Cao, P. & Raleigh, D. P. Analysis of the inhibition and remodeling of islet amyloid polypeptide amyloid fibers by flavanols. *Biochem.* **51**, 2670-2683, (2012).
- 5 Kamihira-Ishijima, M., Nakazawa, H., Kira, A., Naito, A. & Nakayama, T. Inhibitory mechanism of pancreatic amyloid fibril formation: Formation of the complex between tea catechins and the fragment of residues 22–27. *Biochem.* **51**, 10167-10174, (2012).
- 6 Engel, M. F. M. *et al.* The polyphenol EGCG inhibits amyloid formation less efficiently at phospholipid interfaces than in bulk solution. *J. Am. Chem. Soc.* **134**, 14781-14788, (2012).
- 7 Cheng, B. *et al.* Silibinin inhibits the toxic aggregation of human islet amyloid polypeptide. *Biochem. Biophys. Res. Commun.* **419**, 495-499, (2012).
- 8 Bieschke, J. *et al.* EGCG remodels mature  $\alpha$ -synuclein and amyloid- $\beta$  fibrils and reduces cellular toxicity. *Proc. Natl. Acad. Sci. U.S.A.* **107**, 7710-7715, (2010).
- 9 Ehrnhoefer, D. E. *et al.* EGCG redirects amyloidogenic polypeptides into unstructured, off-pathway oligomers. *Nat. Struct. Mol. Biol.* **15**, 558-566, (2008).
- 10 Hyung, S. J. *et al.* Insights into antiamyloidogenic properties of the green tea extract (-)-epigallocatechin-3-gallate toward metal-associated amyloid- $\beta$  species. *Proc. Natl. Acad. Sci. U.S.A.* **110**, 3743-3748, (2013).
- 11 Ferreira, N., Saraiva, M. J. & Almeida, M. R. Natural polyphenols inhibit different steps of the process of transthyretin (TTR) amyloid fibril formation. *FEBS Lett.* **585**, 2424-2430, (2011).
- 12 Hudson, S. A., Ecroyd, H., Dehle, F. C., Musgrave, I. F. & Carver, J. A. (-)-epigallocatechin-3-gallate (EGCG) maintains kappa-casein in its pre-fibrillar state without redirecting its aggregation pathway. *J. Mol. Biol.* **392**, 689-700, (2009).
- 13 Choi, Y.-T. *et al.* The green tea polyphenol (-)-epigallocatechin gallate attenuates  $\beta$ -amyloid-induced neurotoxicity in cultured hippocampal neurons. *Life Sci.* **70**, 603-614, (2001).
- 14 Meng, F., Abedini, A., Plesner, A., Verchere, C. B. & Raleigh, D. P. The flavanol (-)-epigallocatechin 3-gallate inhibits amyloid formation by islet amyloid polypeptide, disaggregates amyloid fibrils, and protects cultured cells against IAPP-induced toxicity. *Biochem.* **49**, 8127-8133, (2010).
- 15 Roterman, I. *et al.* Why Congo red binding is specific for amyloid proteins - model studies and a computer analysis approach. *Med. Sci. Monit.* **7**, 771-784, (2001).
- 16 Khurana, R., Uversky, V. N., Nielsen, L. & Fink, A. L. Is Congo red an amyloid-specific dye? *J. Biol. Chem.* **276**, 22715-22721, (2001).
- 17 Wu, C., Scott, J. & Shea, J.-E. Binding of Congo red to amyloid protofibrils of the Alzheimer A $\beta_{9-40}$  peptide probed by molecular dynamics simulations. *Biophys. J.* **103**, 550-557, (2012).
- 18 Turnell, W. G. & Finch, J. T. Binding of the dye Congo red to the amyloid protein pig insulin reveals a novel homology amongst amyloid-forming peptide sequences. *J. Mol. Biol.* **227**, 1205-1223, (1992).

- 19 Necula, M., Kaye, R., Milton, S. & Glabe, C. G. Small molecule inhibitors of aggregation indicate that amyloid  $\beta$  oligomerization and fibrillization pathways are independent and distinct. *J. Biol. Chem.* **282**, 10311-10324, (2007).
- 20 Lorenzo, A. & Yankner, B. A. Beta-amyloid neurotoxicity requires fibril formation and is inhibited by congo red. *Proc. Natl. Acad. Sci. U.S.A.* **91**, 12243-12247, (1994).
- 21 Pollack, S. J., Sadler, I. I. J., Hawtin, S. R., Taylor, V. J. & Shearman, M. S. Sulfonated dyes attenuate the toxic effects of  $\beta$ -amyloid in a structure-specific fashion. *Neurosci. Lett.* **197**, 211-214, (1995).
- 22 Feng, B. Y. *et al.* Small-molecule aggregates inhibit amyloid polymerization. *Nat. Chem. Biol.* **4**, 197-199, (2008).
- 23 Maltsev, A. S., Grishaev, A. & Bax, A. Monomeric  $\alpha$ -synuclein binds Congo red micelles in a disordered manner. *Biochem.* **51**, 631-642, (2012).
- 24 Meng, F. & Raleigh, D. P. Inhibition of glycosaminoglycan-mediated amyloid formation by islet amyloid polypeptide and proAPP processing intermediates. *J. Mol. Biol.* **406**, 491-502, (2010).
- 25 Harris, J. R. *In vitro* fibrillogenesis of the amyloid  $\beta_{1-42}$  peptide: cholesterol potentiation and aspirin inhibition. *Micron* **33**, 609-626, (2002).
- 26 Thomas, T., Nadackal, T. G. & Thomas, K. Aspirin and non-steroidal anti-inflammatory drugs inhibit amyloid- $\beta$  aggregation. *Neuroreport* **12**, 3263-3267, (2001).
- 27 Lim, G. P. *et al.* Ibuprofen suppresses plaque pathology and inflammation in a mouse model for Alzheimer's disease. *J. Neurosci.* **20**, 5709-5714, (2000).
- 28 McKee, A. C. *et al.* Ibuprofen reduces A $\beta$ , hyperphosphorylated tau and memory deficits in Alzheimer mice. *Brain Res.* **1207**, 225-236, (2008).
- 29 Agdeppa, E. D. *et al.* *In vitro* detection of (S)-naproxen and ibuprofen binding to plaques in the Alzheimer's brain using the positron emission tomography molecular imaging probe 2-(1-{6-[(2-[<sup>18</sup>F]fluoroethyl)(methyl)amino]-2-naphthyl}ethylidene)malononitrile. *Neuroscience* **117**, 723-730, (2003).
- 30 Lockhart, C., Kim, S. & Klimov, D. K. Explicit solvent molecular dynamics simulations of A $\beta$  peptide interacting with ibuprofen ligands. *J. Phys. Chem. B* **116**, 12922-12932, (2012).
- 31 Howlett, D., Cutler, P., Heales, S. & Camilleri, P. Hemin and related porphyrins inhibit  $\beta$ -amyloid aggregation. *FEBS Lett.* **417**, 249-251, (1997).
- 32 Abedini, A. & Raleigh, D. P. Incorporation of pseudoproline derivatives allows the facile synthesis of human IAPP, a highly amyloidogenic and aggregation-prone polypeptide. *Org. Lett.* **7**, 693-696, (2005).
- 33 Abedini, A., Singh, G. & Raleigh, D. P. Recovery and purification of highly aggregation-prone disulfide-containing peptides: Application to islet amyloid polypeptide. *Anal. Biochem.* **351**, 181-186, (2006).
- 34 Nilsson, M. R. & Raleigh, D. P. Analysis of amylin cleavage products provides new insights into the amyloidogenic region of human amylin. *J. Mol. Biol.* **294**, 1375-1385, (1999).
- 35 Nilsson, M. R., Driscoll, M. & Raleigh, D. P. Low levels of asparagine deamidation can have a dramatic effect on aggregation of amyloidogenic peptides: Implications for the study of amyloid formation. *Protein Sci.* **11**, 342-349, (2002).
- 36 Dunkelberger, E. B. *et al.* Deamidation accelerates amyloid formation and alters amylin fiber structure. *J. Am. Chem. Soc.* **134**, 12658-12667, (2012).
- 37 Walsh, D. M. *et al.* A facile method for expression and purification of the Alzheimer's disease-associated amyloid  $\beta$ -peptide. *FEBS J.* **276**, 1266-1281, (2009).